Developmental Cell, Volume *25*

Supplemental Information

Distinct Rap1 Activity States Control the Extent of Epithelial Invagination via α-Catenin

Yu-Chiun Wang, Zia Khan, and Eric F. Wieschaus

Inventory of Supplemental Information

Figure S1, related to Figure 1. Abrogation of an apparent compression force from the posterior pole does not alter the extent of dorsal fold invagination.

Figure S2, related to Figure 2. *α-catenin* RNAi results in a complete loss of α-Catenin protein.

Figure S3, related to Figure 6. An initial requirement of Rap1 function to maintain Bazooka levels can be bypassed with Bazooka overexpression, allowing for the examination of *Rap1* loss-of-function phenotype during dorsal fold invagination.

Movie S1, related to Figure 1. (Part 1) Two photon time-lapse series of the mid-sagittal section view of dorsal fold formation visualized by E-Cadherin-GFP (green) and membrane-mCherry (magenta). (Part 2) Two-photon time-lapse images of the mid-sagittal section view of the dorsal epithelium in a *torso-like* mutant embryo expressing Spider-GFP.

Movie S2, related to Figure 2. (Part 1) Two photon time-lapse series of the mid-sagittal section view of dorsal fold formation in an *α-catenin* RNAi embryo visualized by Resille-GFP. (Part 2) Two photon time-lapse series of the mid-sagittal section view of dorsal fold formation in a *shotgun* RNAi embryo visualized by Resille-GFP.

Movie S3, related to Figure 3. Two photon time-lapse series of the mid-sagittal section view of dorsal fold formation in a RapV12-overexpressing embryo visualized by E-Cadherin-GFP.

Movie S4, related to Figure 4. Two photon time-lapse series of the mid-sagittal section view of dorsal fold formation in a *Rapgap1* mutant embryo visualized by E-Cadherin-GFP.

Movie S5, related to Figure 6. (Part 1) Two photon time-lapse series of the mid-sagittal section view of dorsal fold formation in a Rap1N17-overexpressing embryo visualized by E-Cadherin-GFP. (Part 2) Two photon time-lapse series of the mid-sagittal section view of dorsal fold formation in an embryo that overexpresses both Rap1N17 and Bazooka-GFP visualized by Bazooka-GFP (green) and membrane-mCherry.

Movie S6, related to Figure 4. (Part 1) Two photon time-lapse series of the mid-sagittal section view of dorsal fold formation in a Rapgap1-overexpressing

embryo visualized by E-Cadherin-GFP. (Part 2) Two photon time-lapse series of the mid-sagittal section view of dorsal fold formation in a Rapgap1-overexpressing embryo visualized by E-Cadherin-GFP.

Supplemental Figures

Figure S1

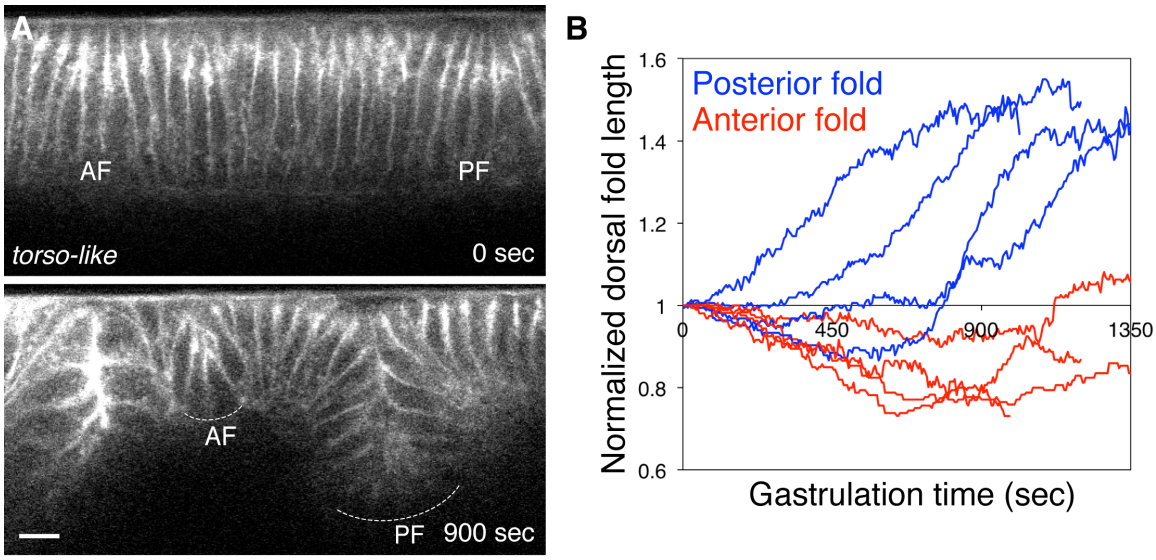

Figure S1, related to Figure 1. Abrogation of an apparent compression force from the posterior pole does not alter the extent of dorsal fold invagination.

(A) Two-photon time-lapse images of the mid-sagittal section view of the dorsal epithelium in a *torso-like* mutant embryo expressing Spider-GFP. AF, anterior fold. PF, posterior fold. (A, see also Movie S1 Part 2) shows the initial junctional shift at the onset of gastrulation (0 sec) and the eventual morphology of the dorsal folds (900 sec). Dashed curves indicate the bottom of the dorsal folds. Scale bar, 10 μm. The *torso-like* mutation disrupts posterior midgut formation, thus preventing the extending lateral germband from exerting compression on the dorsal tissue. The eventual morphology of the dorsal folds appears normal in this mutant background. (B) Total dorsal fold length as a function of time in the *torso-like* mutant embryos. Dorsal fold length was measured as in Figure 1C. The depth of the posterior fold increases to a degree similar to that in the wild-type, indicating that the extensive invagination of the posterior fold does not require the external compression caused by the movement of the posterior midgut during germband extension. The kinetics of the posterior fold lengthening does appear far more variable and inefficient, suggesting that the external compression, although not a deterministic factor of the ultimate morphology, facilitates and ensures a robust invagination.

Figure S2

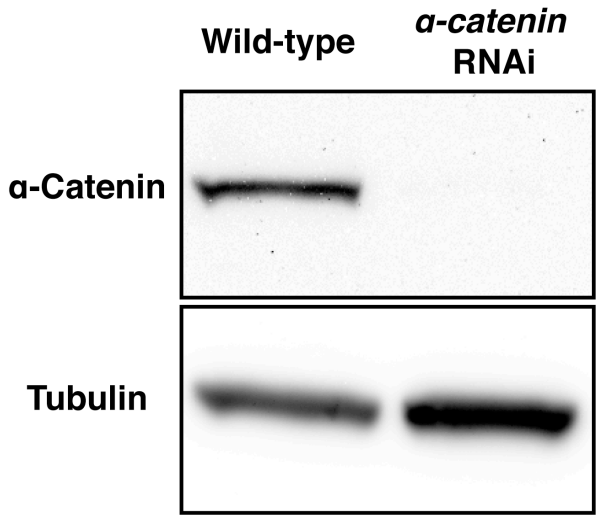

Figure S2, related to Figure 2. *α-catenin* RNAi results in a complete loss of α-Catenin protein.

Western blot analysis of the wild-type and *α-catenin* RNAi embryos shows that α-Catenin protein is undetectable in the *α-catenin* RNAi embryos. Lysate of 40 gastrulating embryos was loaded in each lane. Tubulin immunoblot was used as a control.

Figure S3

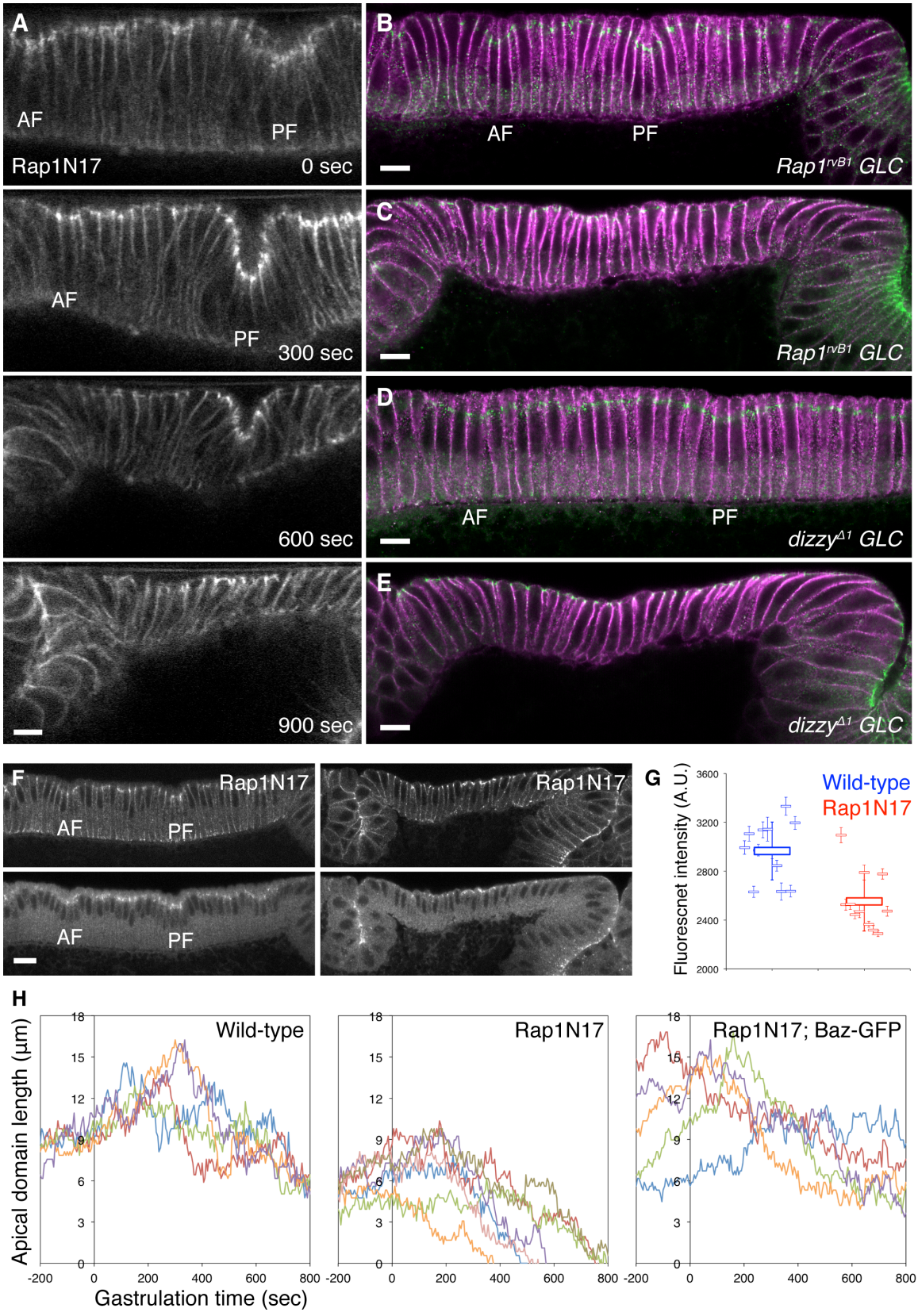
A
AF
PF
Rap1N17
0 sec
B
AF
PF
Rap1rvB1 GLC
AF
PF
300 sec
C
Rap1rvB1 GLC
600 sec
D
AF
PF
dizzyΔ1 GLC
900 sec
E
dizzyΔ1 GLC
F
Rap1N17
AF
PF
Rap1N17
AF
PF
G
Wild-type
Rap1N17
Fluorescnet intensity (A.U.)
3600
3200
2800
2400
2000
H
Wild-type
Rap1N17
Rap1N17; Baz-GFP
Apical domain length (µm)
18
15
12
9
6
3
0
-200
0
200
400
600
800
Gastrulation time (sec)

Figure S3, related to Figure 6. An initial requirement of Rap1 function to maintain Bazooka levels can be bypassed with Bazooka overexpression, allowing for the examination of *Rap1* loss-of-function phenotype during dorsal fold invagination.

(A-E) Adherens junctions undergo apical re-positioning and thereby eliminate dorsal fold structure in embryos that lack active Rap1. **(**A) Two-photon time-lapse images of the mid-sagittal section view of E-Cadherin-GFP in a gastrulating embryo overexpressing Rap1N17 (see also Movie S5 Part 1). (B-E) Confocal images of the mid-sagittal section view of the immunofluorescence of Armadillo (green) and Neurotactin (magenta) in the dorsal epithelium of embryos produced by germline clones homozygous for $Rap1^{rvB1}$ (B and C) or $dizzy^{\Delta 1}$ (D and E) during early (B and D) or late gastrulation (C and E).

(F-G) An early requirement of Rap1 function maintains the junctional levels of Bazooka. (F) Confocal images of the mid-sagittal section view of the immunofluorescence of Armadillo (top panels) and Bazooka (bottom panels) in the dorsal epithelium of embryos expressing Rap1N17 during early (left panels) or late (right panels) gastrulation. AF, anterior fold. PF, posterior fold. Scale bar, 10 μm. (G) Comparison of Bazooka junctional concentration between the wild-type and Rap1N17 embryos. Bazooka concentration was quantified using the immunofluorescent intensity of Bazooka in the junctional region normalized by the junctional volume. Small symbols denote average intensity among 300 to 500 dorsal cells within an embryo; large symbols denote average intensity among the average values of individual embryos. Error bars, standard deviation.

(H) Overexpression of Bazooka in *Rap1* loss-of-function embryos restores the apical domain and dorsal fold structures. The length of apical domain is plotted as a function of time in the wild-type (n = 5), Rap1N17-expressing (n = 7) embryos and RapN17 embryos that overexpress Bazooka-GFP (n = 5).

Movie legends

Movie S1, related to Figure 1.
(Part 1) Two photon time-lapse series of the mid-sagittal section view of dorsal fold formation visualized by E-Cadherin-GFP (green) and membrane-mCherry (magenta). The depth of the two dorsal folds and the number of cells that becomes incorporated into each fold are distinctively different. (Part 2) Two-photon time-lapse images of the mid-sagittal section view of the dorsal epithelium in a *torso-like* mutant embryo expressing Spider-GFP. The *torso-like* mutation disrupts posterior midgut formation, thus preventing the extending lateral germband from exerting an apparent push on the dorsal tissue. The eventual morphology of the dorsal folds, however, appears normal in this mutant background. Scale bar, 10 μm.

Movie S2, related to Figure 2.
(Part 1) Two photon time-lapse series of the mid-sagittal section view of dorsal fold formation in an *α-catenin* RNAi embryo visualized by Resille-GFP. The epithelial structure appears intact during dorsal fold formation and the anterior fold undergoes an extensive invagination, comparable to that of the posterior fold. After dorsal fold formation, a large number of cells become distorted or appear to round up, indicative of loss of cell adhesion. (Part 2) Two photon time-lapse series of the mid-sagittal section view of dorsal fold formation in a *shotgun* RNAi embryo visualized by Resille-GFP. The epithelial structure becomes disorganized during late cellularization and dorsal folds do not form. Scale bar, 10 μm.

Movie S3, related to Figure 3.
Two photon time-lapse series of the mid-sagittal section view of dorsal fold formation in a RapV12-overexpressing embryo visualized by E-Cadherin-GFP. The invagination of the posterior fold is defective. Scale bar, 10 μm.

Movie S4, related to Figure 4.
Two photon time-lapse series of the mid-sagittal section view of dorsal fold formation in a *Rapgap1* mutant embryo visualized by E-Cadherin-GFP. The invagination of the posterior fold is defective. Scale bar, 10 μm.

Movie S5, related to Figure 6.
(Part 1) Two photon time-lapse series of the mid-sagittal section view of dorsal fold formation in a Rap1N17-overexpressing embryo visualized by E-Cadherin-GFP. The junctions undergo a basal shift initially, but subsequently re-localize apically, resulting in the elimination of dorsal fold structure. (Part 2) Two photon time-lapse series of the mid-sagittal section view of dorsal fold formation in an embryo that overexpresses both Rap1N17 and Bazooka-GFP visualized by Bazooka-GFP (green) and membrane-mCherry. The apical domain and the dorsal fold structure are restored, but the invagination of the posterior fold is defective. Scale bar, 10 μm.

Movie S6, related to Figure 4.
(Part 1) Two photon time-lapse series of the mid-sagittal section view of dorsal fold formation in a Rapgap1-overexpressing embryo visualized by E-Cadherin-GFP. Note that the juncitons display an initial basal shift, but undergo a subsequent apical re-localization, resulting in the elimination of dorsal folds. This phenotype is similar to the *Rap1* loss-of-function phenotype (see Movie S7). (Part 2) Two photon time-lapse series of the mid-sagittal section view of dorsal fold formation in a Rapgap1-overexpressing embryo visualized by E-Cadherin-GFP. The phenotype of this embryo is similar to that of the *Rapgap1* loss-of-function embryo (see Movie S6). Scale bar, 10 μm.